# A Study on Modeling of a Surge Protection Device

# A Study on Modeling of a Surge Protection Device

Kohei NAGATOMO[a)], Muhammad Aziz MUSLIM[b)], Hiroki TAMURA[c)]
Koichi TANNO[d)], WIJONO[b)]

## Abstract

This paper presents a modeling of a surge protection device based on V-t curve characteristic. Metal oxide varistor (MOV) is one of common surge protection devices to protect following electric devices from over-voltage such as the lightning and electrostatic discharge (ESD) by controlled the supplied surge voltage. It has been known well that MOV has non-linear characteristic between current and supplied voltage, and the I-V characteristic has been modeled by learning system in earlier papers. This paper focuses on a different characteristic of MOV, supplied voltage and control time. To model the V-t curve, the analysis using multiple regression analysis (MRA) and adaptive network based-fuzzy inference system (ANFIS) will be used with several datasets obtained by a high-voltage experiment concerning to the varistor. The results obtained from those learning systems show the V-t curve has possible to be elements for modeling the varistor as a voltage control device.

*Keywords*: Surge protection device, Metal oxide varistor, V-t curve, MRA, ANFIS

## 1. INTRODUCTION

The development in electronics field has provided new period that various types of electronic devices support our lives. Home electrical appliances, smartphones and personal computers are necessary to make us more comfortable. However, these devices are sometimes broken by natural phenomena such as lightning strikes and electrostatic discharge unexpectedly. The lightning and electrostatic are generally called surge voltages, their voltage values sometimes reach into the tens of thousands volts in a flash. Surge voltages cause insulation breakdowns in the electronic devices due to its extremely high voltage. To protect electronic devices from those breakdowns, surge protection devices (SPDs) have been used widely. SPDs are devices that have voltage clipping capability. 0Therefore, they can adjust surge voltages to be used as standard voltage level for the following components and circuits. As typical examples of SPDs, lightning arrestor and metal oxide varistor (MOV) are given in Fig. 1. The principle of SPDs is like a bypass in the circuit to disperse supplied surge voltages. Although their principles are similar, the use of them depends on the target should be protected. This paper focuses on one of MOVs, zinc oxide varistor (ZOV) that are non-ohmic devices and has nonlinear characteristic between current I and voltage V. Nonlinearity of ZOV has been known as effective way to suppress surge voltages, however, its origin has not been clarified yet. A few papers have proposed modeling of I-V characteristic of ZOV using numerical analysis[1)]. In this paper, some relations of ZOV based on behaviors of surge voltages are verified. Especially, a characteristic between voltage V and time t to suppress surge voltages, V-t curve. To express V-t curve of ZOV, waveforms of surge impulse voltage and suppressed voltages are obtained from a high voltage experiment. Besides, several variables are defined as actual data for expressing characteristics. For the modeling of V-t curve, analysis based on some prediction system, multiple regression analysis (MRA) and adaptive neuro fuzzy inference system (ANFIS) are performed. Finally comparison of characteristic of actual data obtained from high voltage experiment and predicted data obtained by prediction systems is given to establish the model of ZOV.

Fig. 1 Surge Protection Devices (Arrestor & MOV)

## 2. METAL OXIDE VARISTOR

### 2.1 Construction and principle

Metal oxide varistor is a voltage dependant resistor in which the resistance material is a metallic oxide, primarily zinc oxide (ZnO) pressed into a ceramic material[2-3)]. Metal oxide varistors consist of approximately 90% zinc oxide as a ceramic base material plus other filler materials for the formation of

a)Master Student, Dept. of Electrical and Electronic Engineering
b)Lecturer, Dept. of Electrical Engineering, University of Brawijaya, Indonesia.
c)Associate Professor, Dept. of Environmental Robotics
d)Professor, Dept. of Electrical and Systems Engineering

junctions between the zinc oxide grains as shown in Fig. 2.

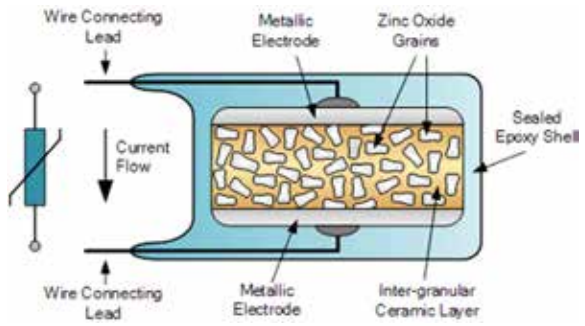


Fig. 2. Configuration of ZOV

Metal oxide varistors are now the most common type of voltage clamping device and are available for use as ta wide range of voltages and currents. The use of a metallic oxide within their construction means that MOV's are extremely effective in absorbing short-term voltage transients and have higher energy handling capabilities. As with the normal varistor, the metal oxide varistor starts conduction at a specific voltage and stops conduction when the voltage falls below a threshold voltage. The main differences between a standard silicon carbide (SiC) varistor and MOV type varistor is that the leakage current through the MOV's zinc oxide material is very small at normal operating conditions and its speed of operation in clamping transients is much faster.

## 2.2 I-V characteristic

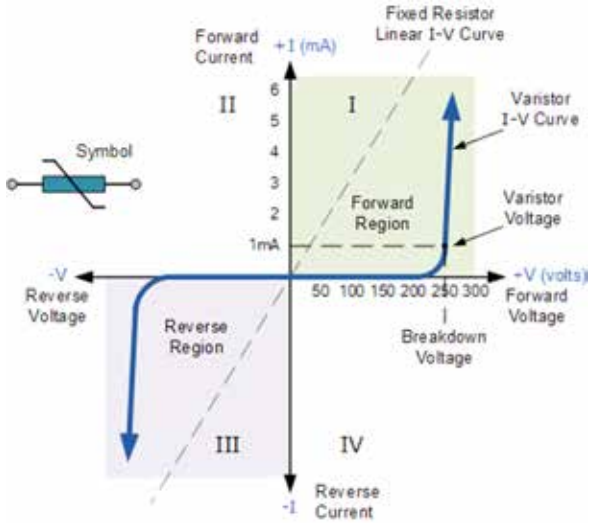


Fig. 3. I-V curve of ZOV

Fig. 3 shows symmetrical bi-directional characteristics of ZOV; the varistor operates in both directions (quadrant I and III) of a sinusoidal waveform behaving in a similar way to two zener diodes connected back to back. When not conducting, the I-V curve shows a linear relationship as the current flowing through the varistor remains constant and low at only a few micro-amperes of leakage current. This is due to high resistance of varistor acting as an open circuit and remains constant until the voltage across the varistor reaches a particular "rated voltage".

This rated or clamping voltage is the voltage across the varistor measured with the specified DC current of 1mA. That is, the DC voltage level applied across its terminals that allows a current of 1mA to flow through the varistors resistive body which itself is dependant upon the materials used in its construction. At this voltage level, the varistor beings to change from its insulating state into its conducting state.

When the transient voltage across the varistor is equal to or greater than the rated voltage, the resistance of the device suddenly becomes very small turning the varistor into a conductor due to the avalanche effect of its semiconductor material. The small leakage current flowing through the varistor rapidly rises but the voltage across it is limited to a level just above the varistor voltage. In other words, the varistor self-regulates the transient voltage across it by allowing more current to flow through it and because of its steep nonlinear I-V curve it can pass widely varying currents over a narrow voltage range clipping-off any voltage spikes. A number of earlier papers perform a challenge to simulate the nonlinear I-V curve of MOV with numerical analysis.

# 3. HIGH VOLTAGE EXPERIMENT

## 3.1 Experimental conditions

High voltage experiment is performed to see the behavior of impulse voltage generated by impulse voltage generator shown in Fig. 4 as circuit diagram. Explanations of each device included in the generator are given in Table 1.

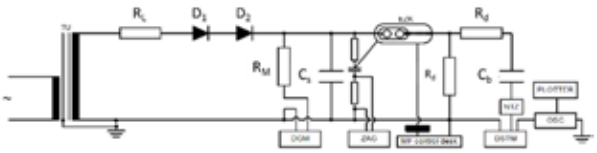

Fig. 4. Impulse voltage generator

Table 1. Description of devices

| Device | Description |
|---|---|
| TU | High voltage Transformer |
| DGM | Digital Measurement Instrument |
| DSTM | Impulse Voltmeter |
| ZAG | Triggering Instrument |
| EZK | Electronic Triggering Sphere |
| NTZ | Low Voltage Divider |
| OSC | Oscilloscope |

DC voltage in the range of 3.0 to 10 kV with 0.5 kV step are supplied to the generator and impulse

voltages are generated by transforming DC voltages. A voltage applied to a capacitor $C_0$ is measured in this experiment and ZOV is connected it in parallel. ZOV here has 10 mm rounded electrodes and 680 V of threshold voltage generally called varistor voltage.

By pushing a trigger button on the control box, impulse voltages are generated between two electronic triggering spheres and indicated as the waveform in the oscilloscope. This experiment was conducted two times, in February and March 2014.

### 3.2 Behavior of impulse voltage

Two kinds of impulse voltage are obtained at every DC voltage step; one is simple impulse voltage depicted in Fig. 5 generated by the generator not including ZOV and the other is controlled impulse voltage depicted in Fig. 6 obtained from the generator including ZOV. As mentioned before, both waveforms are measured at capacitor $C_0$. Comparing Fig 6 to Fig. 5, it can be seen a peak voltage of simple impulse voltage is controlled by including ZOV in the generator.

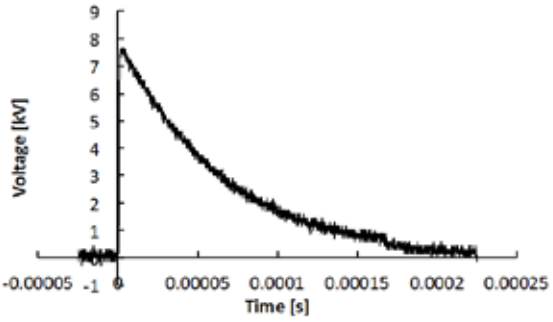


Fig. 5. Simple impulse voltage at DC 10 kV

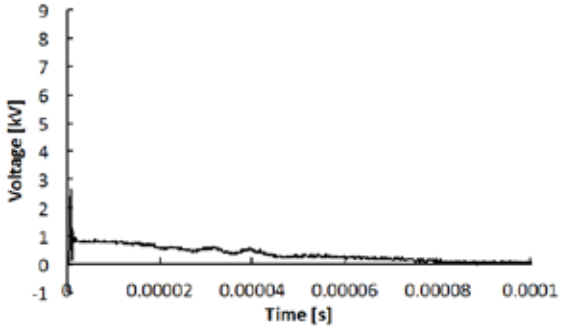


Fig. 6. Controlled impulse voltage

## 4. DISCUSSION

### 4.1 Definition of parameters

From two kinds of waveforms of simple and controlled impulse voltages, several parameter are defined as actual parameters in Fig. 7 and Fig. 8. $V_{imp}$ and $T_{half}$ depicted in Fig. 7 show a peak voltage and time when the peak falls to 50%. In Fig. 8, $V_{max}$, $V_{min}$, $T_{max}$ and $T_{min}$ represent peak voltage, minimal voltage and time at $V_{max}$ and $V_{min}$, respectively.

In addition, $V_{imp}$ and $T_{half}$ are handled as input factor, and $V_{max}$, $V_{min}$, $T_{max}$ and $T_{min}$ are used as output factor.

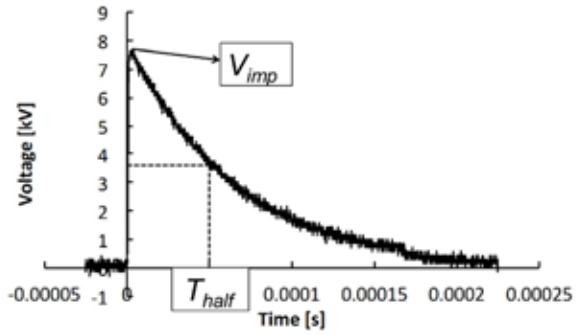


Fig. 7. Definition of $V_{imp}$ and $T_{half}$

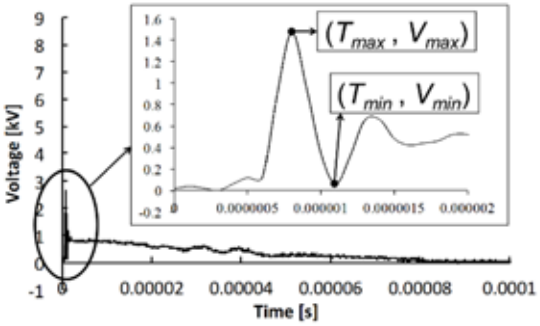


Fig. 8. Definition of $V_{max}$, $V_{min}$, $T_{max}$ and $T_{min}$

### 4.2 Characteristic between actual parameters

This subsection presents some examinations of relationship between actual parameters especially based on $V_{max}$, $V_{min}$ and $T_{max}$ and $T_{min}$ related to $V_{imp}$. Fig. 9 and 10 show relations between actual $V_{max}$ and $V_{imp}$, $V_{min}$ and $V_{imp}$, respectively.

From figures above, actual $Vmax$ shows direct proportion to $V_{imp}$ and $V_{min}$ shows inverse proportion to $V_{imp}$. Furthermore, both approximate function has high coefficient of determination. Therefore, it also can be said both of them have strong linearity. Fig. 11 and 12 show V-t curve based on actual $V_{imp}$, $T_{max}$ and $T_{min}$.

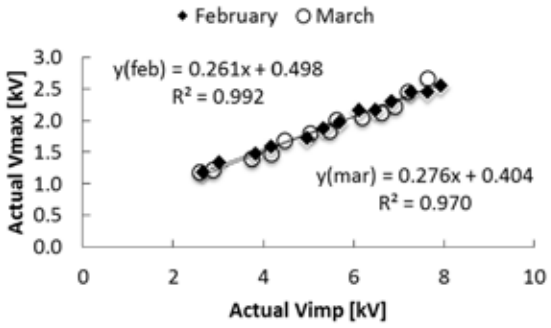


Fig. 9. Actual $V_{max}$ - $V_{imp}$

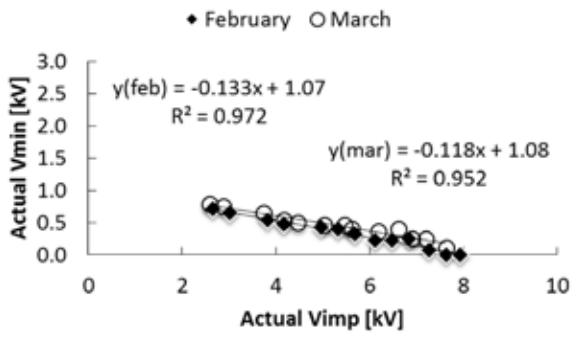


Fig. 10. Actual Vmin - Vimp

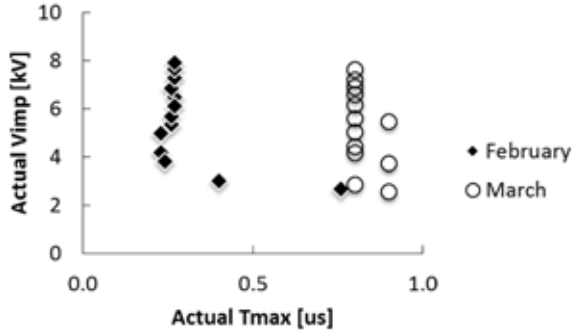


Fig. 11. Actual Vimp - Tmax

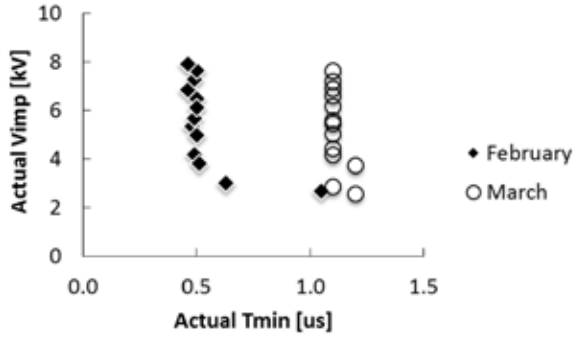


Fig. 12. Actual Vimp - Tmin

Considering Fig. 11 and 12, almost every plot are invariable except some of them and there are difference between every experimental date, though the experimental condition is same on both days. Therefore, those differences may be occurred by another factor, this paper couldn't reach to find out the reason.

## 5. ANALYSIS WITH MULTIPLE REGRESSION ANALYSIS

### 5.1 Multiple regression analysis

Multiple regression analysis is a useful technique for predicting the unknown value from two or more known values. An example of dataset is given in Table 2.

Table 2. Example of MRA

| No. | Weight [kg] | Height [cm] | Chest [cm] |
|---|---|---|---|
| 1 | $W_1$ | $H_1$ | $C_1$ |
| 2 | $W_2$ | $H_2$ | $C_2$ |
| 3 | $W_3$ | $H_3$ | $C_3$ |

When the value of weight is predicted from height and chest, weight is explained in an equation as below and the target of prediction, the value of weight, is called dependent variable, the value of height and chest are independent (exploratory) variables.

$$W = c + aH + bC \quad (1)$$

Here $c$ is an intercept, $a$ and $b$ are analogous to the slope in linear regression equation and are also called regression coefficients which can indicate the influence on the value of weight. As another index which indicate how good the regression is, coefficient of determination defined as $R^2$ which has the value from 0 to 1. The value of $R^2$ approaches 1, it can be said the regression equation provide good prediction results. Each defined variables, $V_{max}$, $T_{max}$, $V_{min}$ and $T_{min}$, are predicted one by one from two independent variables, $V_{imp}$ and $T_{half}$. The number of data in one variable is thirteen data.

### 5.2 Result

Through the analysis using MRA, the regression equation and coefficient of determination corresponding each independent variable are obtained. In addition, predicted $V_{max}$, $T_{max}$, $V_{min}$ and $T_{min}$ are compared with actual data of them.

At first, the regression equations and coefficient of determination $R^2$ are described in Table 3.

Table 3. Regression equation of each parameter

| Experimental Date | Target | Regression equation | $R^2$ |
|---|---|---|---|
| February 2014 | Vmax | Vmax = 0.59 + 0.27 Vimp - 0.0026 Thalf | 0.99 |
| | Tmax | Tmax = 1.9+ 0.014 Vimp - 0.038 Thalf | 0.75 |
| | Vmin | Vmin = 0.97 + 0.14 Vimp + 0.0028 Thalf | 0.97 |
| | Tmin | Tmin = 2.2 + 0.0006 Vimp - 0.037 Thalf | 0.75 |
| March 2014 | Vmax | Vmax = 0.49 + 0.28 Vimp - 0.0032 Thalf | 0.97 |
| | Tmax | Tmax = 0.79 + 0.021 Vimp + 0.0036 Thalf | 0.33 |
| | Vmin | Vmin = 1.1 + 0.11 Vimp - 0.0018 Thalf | 0.95 |
| | Tmin | Tmin = 1.1 + 0.021 Vimp + 0.0031 Thalf | 0.44 |

From the results of each regression equations, both of $V_{max}$ and $V_{min}$ obtained in February and March are expressed as equations with high coefficient of determination $R^2$ and those regression equation are influenced by $V_{imp}$. However, regression equations of $T_{max}$ and *Tmin* show different characteristic. In the results of February, regression equations of $T_{max}$ and $T_{min}$ are strongly affected by $T_{half}$ than $V_{imp}$ as seen from differences of coefficients. By contrast, in the results of March, coefficient of $V_{imp}$ is larger than coefficient of $T_{half}$. In other words, $T_{max}$ and *Tmin* may have another factor to be affected.

As additional results, relations between actual and predicted value of each variable are shown in Fig.13 to Fig.16.

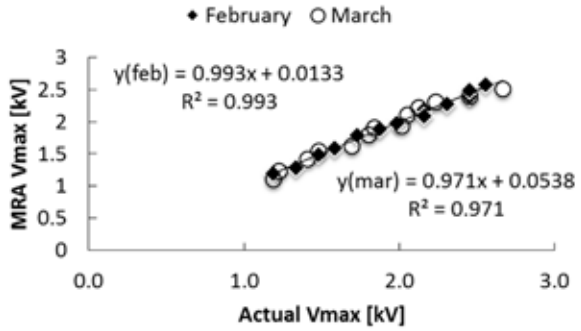


Fig. 13. Relation between $V_{max}$ of actual and MRA

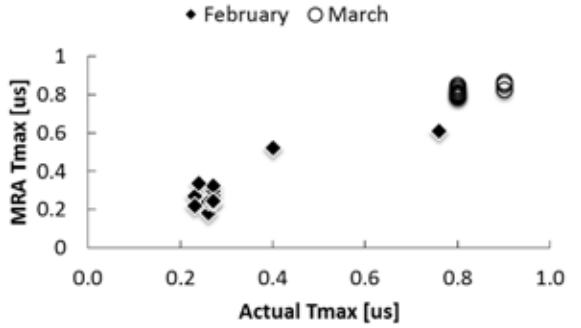


Fig. 14. Relation between $T_{max}$ of actual and MRA

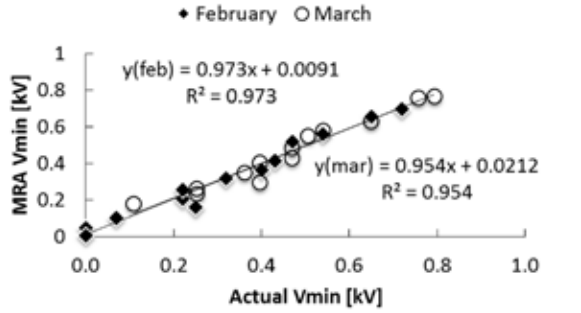


Fig. 15. Relation between $V_{min}$ of actual and MRA

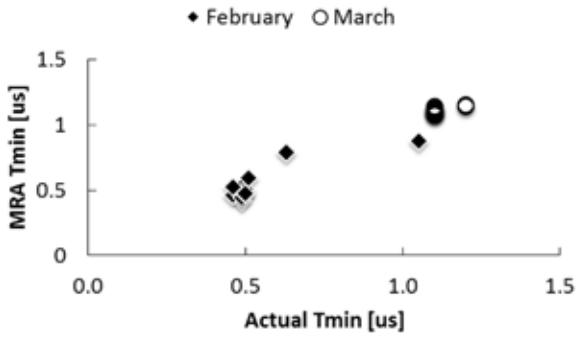


Fig. 16. Relation between $T_{min}$ of actual and MRA

The results in Fig.13 and Fig.15 indicate that a strong linearity and high prediction accuracy can be seen from actual and predicted values in case of $V_{max}$ and $V_{min}$. Results of $T_{max}$ and $T_{min}$ behave like constant rather than having the nonlinearity.

## 6. ANALYSIS WITH ADAPTIVE NEURO FUZZY INFERENCE SYSTEM

### 6.1 Adaptive neuro fuzzy inference system

Adaptive network-based-fuzzy inference system (ANFIS) is an effective learning system combined fuzzy inference system and framework of adaptive networks[4]. The ANFIS provides a construction of input-output mapping based on human knowledge and is excellent in non-linear prediction. Fig.17 shows ANFIS architecture proposed by Jang.

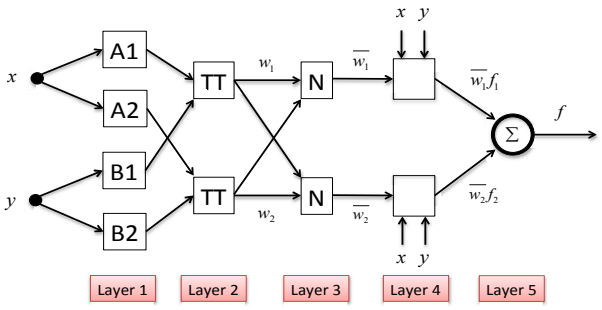


Fig. 17. ANFIS architecture

ANFIS here consists of one output from two input data and Takagi and Sugeno's if-then rules[5] depicted in Fig. 18 are allowed in the learning step.

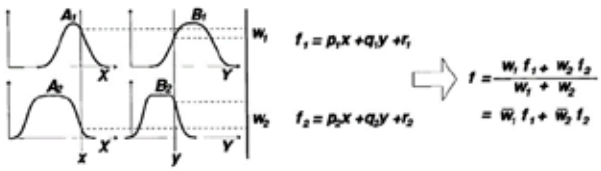

Fig. 18. Takagi and Sugeno's fuzzy rule

ANFIS used in this paper has five layers described as below;

**Layer 1**: Each node *i* in this layer is a square node with a node function;

$$O_i^1 = \mu_{A_i}(x) \tag{2}$$

where x is the input to node *i*, and $A_i$ is the linguistic label such as small and large associated with this node function. $O^1_i$ is also called membership function and it specifies the degree to which the given x satisfies the quantifier $A_i$. The membership function is usually defined as a bell-shaped function;

$$\mu_{A_i}(x) = \frac{1}{1 + \left[\left(\frac{x - c_i}{a_i}\right)^2\right]^{b_i}} \tag{3}$$

where $\{a_i, b_i, c_i\}$ is the parameter set.

**Layer 2**: Each node in this layer conducts the multiplication of the incoming signals and sends the product out.

$$w_i = \mu_{A_i}(x) \times \mu_{B_i}(y), \quad i = 1,2. \tag{4}$$

Outputs of this layer indicate the firing strength of a rule.

**Layer 3**: Calculating the ratio of the *i* th rule's firing strength to the sum of all rule's firing strength is conducted.

$$\overline{w_i} = \frac{w_i}{w_1 + w_2}, \quad i = 1,2. \tag{5}$$

**Layer 4**: Parameters called consequent parameters are obtained from the equation

$$O_i^4 = \overline{w_i} f_i = \overline{w_i}(p_i x + q_i y + r_i), \quad i = 1,2. \tag{6}$$

Where $\overline{w_i}$ is the output of layer 3, and $\{p_i, q_i, r_i\}$ is the parameter set.

**Layer 5**: This layer computes the overall output as the summation of all incoming signals.

$$O_i^5 = \sum \overline{w_i} f_i = \frac{\sum_i w_i f_i}{\sum_i w_i} \tag{7}$$

In this paper, local search learning for parameters {***a, b, c***} and {***p, q, r***} are employed, and the local search provide a higher probability in the ANFIS.

## 6.2 Conditions of ANFIS

ANFIS here provides one predicted value of $V_{max}$, $T_{max}$, $V_{min}$ or $T_{min}$, as an output from two input data, $V_{imp}$ and $T_{half}$, respectively. Both of input have thirteen data. Four bell-shaped function are used as membership function whose initial parameters are defined as $a = 0.5$, $b = 1$ and $c = 5$ in each input nodes. Final predicted value will be obtained when the average of error becomes the smallest value.

## 6.3 Results

In the same way of MRA, relations between actual and predicted data will be shown in Fig. 19 to 22. As can be seen from Fig. 19 and Fig. 21, although the value of $R^2$ is smaller than results of MRA, relations between actual and predicted data in $V_{max}$ and $V_{min}$ has strong linearity. Results from Fig. 20 and Fig. 22, most of plots are gathering in an area. It also can be said predicted time may be constant.

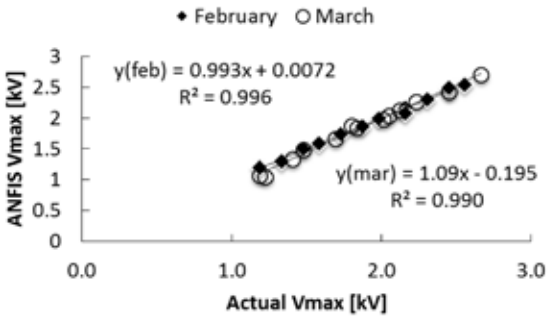


Fig. 19 Relation between $V_{max}$ of Actual and ANFIS

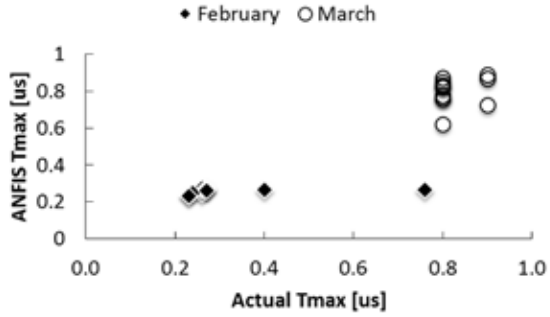


Fig. 20 Relation between $T_{max}$ of Actual and ANFIS

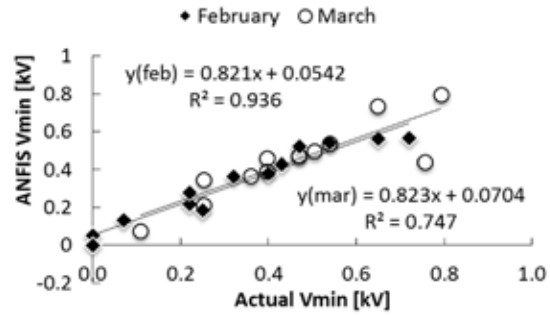


Fig. 21 Relation between $V_{min}$ of Actual and ANFIS

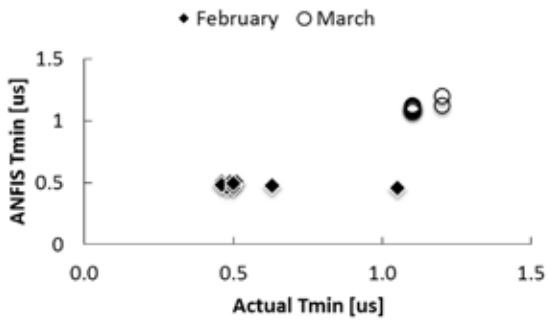


Fig. 22 Relation between $T_{min}$ of Actual and ANFIS

## 7. V-t CURVE MODELING

### 7.1 Comparison of RMSE

Prediction accuracy of both predictor is confirmed by observing root mean square error (RMSE). In Fig. 23 to 25, RMSE of MRA and ANFIS are compared to show prediction accuracy. MRA results lower RMSE and variance than ANFIS except Vmax. Therefore, it is more effective for modeling V-t curve of ZOV to employ MRA's regression equations.

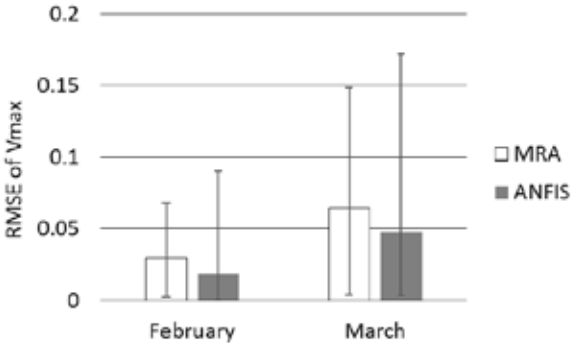


Fig. 23 RMSE of $V_{max}$

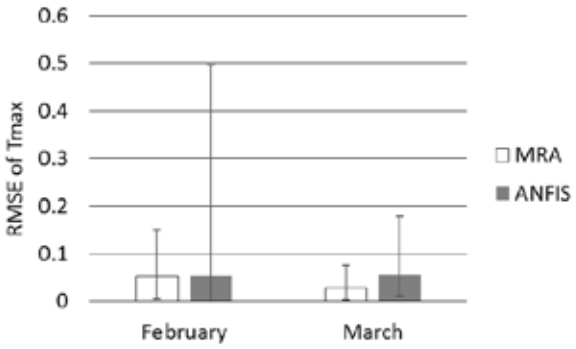


Fig. 24 RMSE of Tmax

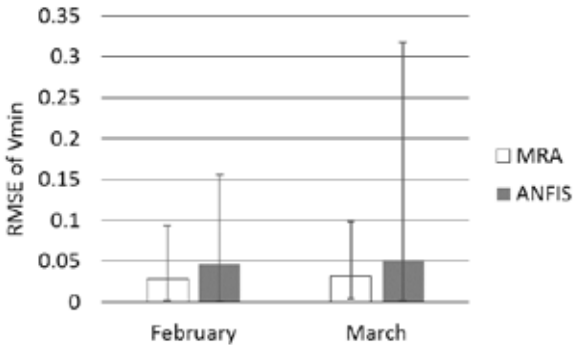


Fig. 25 RMSE of $V_{min}$

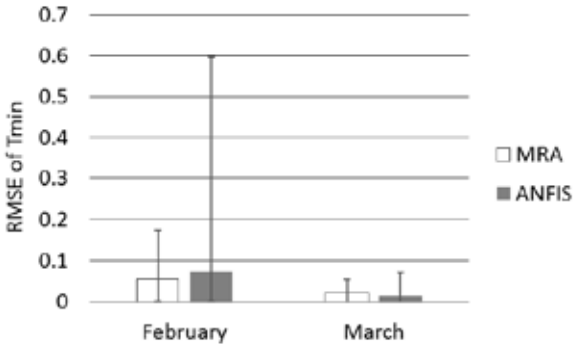


Fig. 26 RMSE of $T_{min}$

### 7.2 Modeled V-t curve

Considering lower RMSE and variance, it can be thought V-t curve of ZOV should be modeled by MRA's regression equations described in Table 3. Here some cautions are required to model V-t curve. This paper would like to present modeled V-t curve only based on input-output relations; only two relationships between actual $V_{imp}$ and predicted $T_{max}$, and relation between actual $V_{imp}$ and predicted $T_{min}$. As considerable pattern of combination of voltage and time parameters, relationship between actual $V_{imp}$ and predicted time $T_{max}$ and $T_{min}$ obtained from MRA are observed in Fig. 27 and 28.

From Fig. 27 and 28, it can be seen that there significant differences between result of February and March. In both of V-t curves based on $V_{imp}$ - $T_{max}$ and $V_{imp} - T_{min}$, result of February shows curved line, on the other hand, function line of March is relatively straight and linear. From result of V-t curve, it can be said there is possibility that another factor have influence on the V-t curve. However, this paper could not reach to detect definite answer for the reason.

Conducting experiment with another condition and confirming of repeatability of obtained parameter are required to improve this paper.

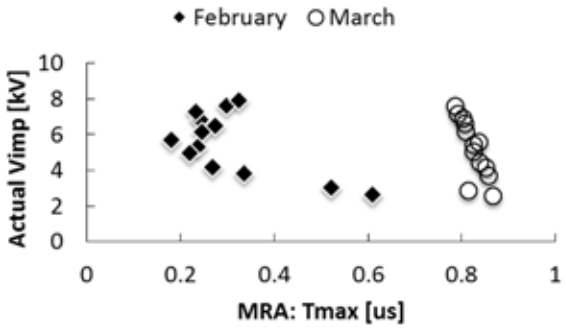


Fig. 27 Modeled V-t curve ($V_{imp}$ – predicted $T_{max}$)

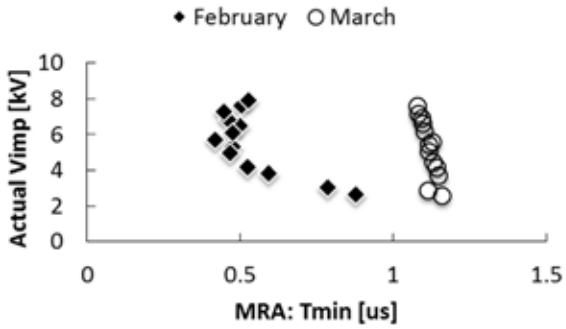


Fig. 28 Modeled V-t curve ($V_{imp}$ – predicted $T_{min}$)

## 8. CONCLUSION

In this paper, characteristic of ZOV based on V-t curve has been model by using actual and predicted data obtained from high voltage experiment and two kinds of learning system, respectively. In high voltage experiment, impulse voltage was generated by using impulse voltage generator. Each of DC voltages which have range of 3.0 to 10 kV with 0.5 kV step is applied to the generator, simple impulse voltage and controlled impulse voltage were obtained from generator not including and including ZOV. Waveforms of simple and controlled impulse voltage was recorded by oscilloscope, $V_{imp}$ and $T_{half}$ were defined in the waveform of simple impulse voltage, then $V_{max}$, $T_{max}$, $V_{min}$ and $T_{min}$ were defined from the controlled impulse voltage. By considering some relations between actual data, a strong linearity was confirmed by graph considering $V_{imp}$ and two of actual voltage, $V_{max}$ and $V_{min}$. In the prediction using two kinds of learning system, multiple regression analysis (MRA) and adaptive neuro fuzzy inference system (ANFIS), predicted $V_{max}$, $T_{max}$, $V_{min}$ and $T_{min}$ were derived, both of learning systems have provided high accuracy in the predicting. $V_{max}$ and $V_{min}$. Especially, predicted $V_{max}$ and $V_{min}$ obtained from MRA showed higher coefficients of determination $R^2$ than results of ANFIS. Thus, unknown $V_{max}$ and $V_{min}$ can be expressed by MRA's regression equations. As the final step, V-t curve consisting of actual $V_{imp}$ obtained from the high voltage experiment and $T_{max}$ and *Tmin* predicted by MRA was modeled. It was revealed that the predicted $T_{max}$ and $T_{min}$ shows different characteristic in every experimental data. Characteristic of actual actual $V_{imp}$, MRA's $T_{max}$ and $T_{min}$ obtained from experimental data in February seemed that it has nonlinearity. However, this paper could not decide that V-t curve is nonlinear or linear.

To get characteristic in the relation between simple impulse voltage $V_{imp}$ and predicted time $T_{max}$ and $T_{min}$, it will be required to adjust the parameter in the learning system and increase the number of actual data.

## REFERENCES

1) Mohammad R. Meshkatoddini, Steven Boggs, Investigation of the statistical behavior of thin ZnO-based varistors using a Monte Carlo Algorithm, ICEE2006, 14th IranianConference on Electrical Engineering, 16-18 May 2006.

2) J. D. Harnden Jr., F. D. Martzlo, W. G. Morris and F. B. Golden," Metal-oxide varistor: a new way to suppress transients,", Reprint of reprint from Electronics, 1972.

3) Mohammad Reza Meshkatoddini, "Metal Oxide ZnO-Based Varistor Ceramics, “Advances in Ceramics - Electric and Magnetic Ceramics, Bioceramics, Ceramics and Environment, Prof. Costas Sikalidis (Ed.), ISBN:978-953-307-350-7, InTech, 2011.

4) J.R. Jang, ANFIS: adaptive-network-based fuzzy inference system, IEEE Trans. Syst Man Cybern Vol.23, No.3, pp.665-685, 1993.

5) T. Takagi and M. Sugeno, "Fuzzy identification of systems and its applications to modeling and control,", IEEE Trans. SST., Man, Cybern., vol. 15, pp. 116-132, 1985.